Journal of Alloys and Compounds 509 (2011) 7808–7813

Contents lists available at ScienceDirect

Journal of Alloys and Compounds

journal homepage: www.elsevier.com/locate/jallcom

Charge transport and recombination in dye-sensitized solar cells based on hybrid films of TiO_2 particles/TiO_2 nanotubes

Peng Zhong [a], Wenxiu Que [a,*], Jin Zhang [a], Qiaoying Jia [a], Wenjuan Wang [a], Yulong Liao [a], X. Hu [b,*]

[a] Electronic Materials Research Laboratory, School of Electronic and Information Engineering, Xi'an Jiaotong University, Xi'an 710049, Shaanxi, People's Republic of China
[b] School of Materials Science and Engineering, Nanyang Technological University, Nanyang Avenue, Singapore 639798, Singapore

ARTICLE INFO

Article history:
Received 3 January 2011
Received in revised form 6 May 2011
Accepted 7 May 2011
Available online 17 May 2011

Keywords:
Dye-sensitized solar cell
TiO_2 nanotube
Electrochemical impedance spectroscopy
Energy conversion efficiency

ABSTRACT

In this paper, anodic TiO_2 nanotubes are blended into the TiO_2 mesoporous films based on P25 nanoparticles to assemble a list of dye-sensitized solar cells (DSSCs) with different nanotube concentrations. The electron properties of transport and recombination in the fabricated DSSCs are studied by using electrochemical impedance spectroscopy and the open-circuit voltage decay technique under AM 1.5 illumination. Results indicate that the electron lifetime increases with increasing the concentration of the anodic TiO_2 nanotubes, the electron transport time at a blending level of 10 wt% TiO_2 nanotubes is short as compared to that at 0 wt%, and above 10 wt%, the electron transport time has a trend of becoming large. Due to the combining effects of the electron transport and recombination, the electron collecting efficiency and the electron diffusion length obtain maxima at a blending level of 10 wt% nanotubes, which results in a highest short circuit current and a maximum energy conversion efficiency at this point in the DSSCs. This study gives a clear explanation for the performance enhancement of TiO_2 particle-based DSSCs at a blending level of 10 wt% anodic TiO_2 nanotubes and for the performance decrease at a blending level over 10 wt% anodic TiO_2 nanotubes from the angle of the electron transport and recombination. This study also supplies a feasible and easy way to improve the performance of particle-based DSSCs by restraining electron recombination and accelerating electron transportation.

1. Introduction

Dye-sensitized solar cells are of great interest as a potential alternative to conventional silicon solar cells due to their low cost, high energy conversion efficiency and easy fabrication processes [1,2]. The photoanode of DSSCs usually consists of a mesoporous film based on interconnected anatase TiO_2 nanoparticles, sensitized by a monolayer of dye molecules. Upon illumination, the photo-excited dye injects an electron into the conduction band of TiO_2. The electrons diffuse through the TiO_2 network to be collected at the transparent electrode substrate. The light-excited dye is subsequently regenerated electrochemically through an electrolyte, for example, an iodide/triiodide redox couple.

While one of the important features of DSSCs is the mesoporous film of interconnected TiO_2 nanoparticles, which can supply large surface areas for adsorption of a large amount of dye molecules, the performance of DSSCs is still limited by the electron transport in the nanocrystal boundaries and the electron recombination with the electrolyte during the electron migration process. Many researchers have reported that one-dimensional (1D) nanostructures [3–10] can be used in DSSCs in place of nanoparticles to facilitate the electron transferring. In addition to the unique electron properties, the 1D TiO_2 nanostructures have another function as light scattering materials with minimum sacrifice of the surface areas. The 1D TiO_2 nanostructures can either be fabricated perpendicular to the transparent electrode substrate [3–7] or randomly distributed during fabricating the TiO_2 photoanode based on nanoparticles [8–10]. Although the ordered TiO_2 nanostructures perpendicular to substrates can be more helpful for electron transport, the fabrication of these nanostructures in large area is still practically challenging. Thus, it is advantageous to fabricate randomly distributed 1D nanostructure-based DSSCs by doctor-blade or screen printing methods. Besides, the fabricated 1D TiO_2 nanostructures can be added into the nanoparticle system to take the advantages of combining both nanomaterials.

In this work, we studied DSSCs fabricated by blending anodic TiO_2 nanotubes into TiO_2 mesoporous films based on commercial P25 nanoparticles. The electron properties of transport and recombination in the TiO_2 photoanodes with different concentrations of the anodic TiO_2 nanotubes are investigated by electrochemical impedance spectroscopy (EIS) and open-circuit voltage decay (OCVD) measurements under AM 1.5 illumination. Effects of the electron properties of transport and recombination on the performances of DSSCs are also discussed. The novelty lies in the

* Corresponding authors. Tel.: +86 29 82668679; fax: +86 29 82668794.
E-mail addresses: wxque@mail.xjtu.edu.cn (W. Que), asxhu@ntu.edu.sg (X. Hu).

0925-8388/$ – see front matter © 2011 Elsevier B.V. All rights reserved.
doi:10.1016/j.jallcom.2011.05.028

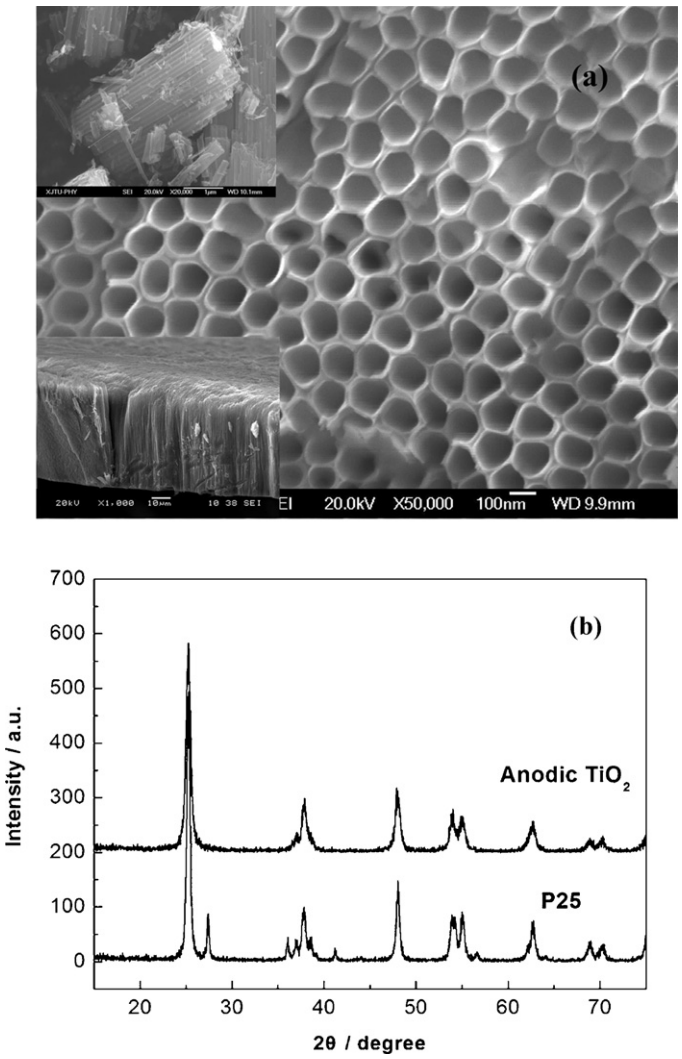

Fig. 1. (a) SEM image of the morphology of the as-anodized TiO_2 nanotube arrays for 3-h anodization, the insert at the bottom left is the cross-sectional image of the as-anodized TiO_2 nanotube arrays, the insert at the top left is the SEM image of the anodic TiO_2 nanotubes after sonification and grinding; (b) XRD patterns of the P25 powder and the anodic TiO_2 nanotube powder after calcination at 450 °C.

investigation of searching the essential reasons for performance improvement and deterioration in DSSCs based on hybrid films of TiO_2 particles/TiO_2 nanotubes.

2. Experimental

2.1. Fabrication of anodic TiO_2 nanotube powders

The fabrication of the anodic TiO_2 nanotube arrays was based on a modified procedures described by Grimes et al. [11–15]. The main processes were depicted as follows: (1) pure Ti sheets (>99.6%, Beijing Nonferrous Metal Research Institute) were cut into small pieces (2 cm × 3 cm), subsequently cleaned in sonification baths at a sequence of acetone and ethanol each for 10 min, and then dried at room temperature. (2) The anodic oxidation was carried out in a two-electrode configuration. The Ti sheet fixed on a copper rod was used as the anode, and the cathode was a larger piece of Ti sheet (3 cm × 5 cm). The electrolyte consisted of 294 ml glycol, 6 ml H_2O and 1 g NH_4F. The whole anodization lasted 3 h at 60 V at room temperature. Thus, highly ordered TiO_2 nanotube arrays can be obtained and attached to the Ti sheet.

In order to obtain powders, the fabricated TiO_2 nanotube arrays had to be detached from the Ti sheet in a water bath under sonification. The anodic oxidation and sonification were repeated many times to obtain the required amount of nanotube powders. Then the white mixture of TiO_2 in water was heated at 100 °C for several hours to evaporate water, and subsequently calcinated at 450 °C for 4 h. Finally the samples were grinded in a mortar.

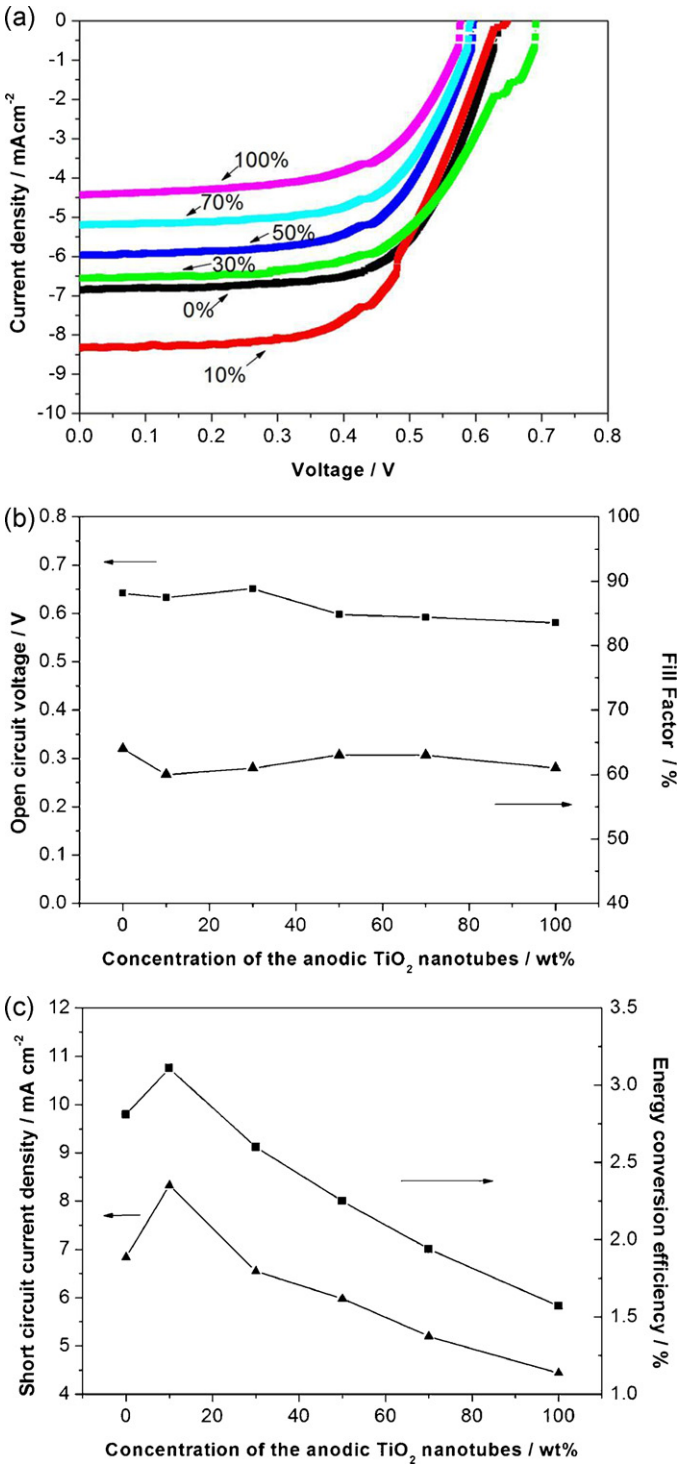

Fig. 2. (a) Current–voltage curves of the DSSCs as a function of the concentration of the anodic TiO_2 nanotubes; (b) curves of open circuit voltage and fill factor as a function of the concentration of the anodic TiO_2 nanotubes; (c) curves of short circuit current and energy conversion efficiency as a function of the concentration of the anodic TiO_2 nanotubes.

2.2. Assembly of DSSCs

SnO_2:F (FTO) transparent conducting glasses were used as the electrode for collecting electrons. A thin TiO_2 blocking layer was first deposited by spin coating a TiO_2 sol onto the FTO substrate, and then calcinated at 450 °C for 1 h. The components of the TiO_2 sol was based on the following formulation [16]: $Ti[O(CH_2)_3CH_3]_4$:H_2O:HCl:CH_3CH_2OH = 1:1.5:0.05:50. The mixture of the P25 nanoparticles with the anodic TiO_2 nanotube powders were first grinded for 20 min, and secondly a mixture of ethyl cellulose and terpineol (component ratio: 50 g ethyl

Table 1
Photovoltaic parameters of the DSSCs.

Samples	V_{oc} (V)	I_{sc} (mA cm^{-2})	FF (%)	Efficiency (%)
0 wt%	0.64	6.84	64	2.81
10 wt%	0.63	8.33	60	3.11
30 wt%	0.65	6.55	61	2.60
50 wt%	0.60	5.98	63	2.25
70 wt%	0.60	5.20	63	1.94
100 wt%	0.58	4.44	61	1.57

cellulose in 950 ml terpineol) was added for further grinding for another 20 min. The obtained pastes were screen printed onto the TiO_2 blocking layer on the FTO substrates with an active area of 0.25 cm^2, and then heat treated at 200 °C for 4 h before being calcinated at 450 °C for 4 h at a heating rate of 5 °C/min. The calcined TiO_2 mesoporous films deposited on FTO substrates were dyed by soaking for 24 h at room temperature in 0.5 mM solutions in absolute ethanol of the ruthenium complex Ru[LL′-(NCS)2] (N-719, L = 2, 2′-bypyridyl-4, 4′-dicarboxylic acid, L′ = 2, 2′-bypyridyl-4, 4′-ditetrabutylalmmoniumcarboxylate]). The Pt counter electrodes were obtained by sputtering Pt onto the FTO substrates. The DSSCs package processes were similar to those as reported previously [17]. The electrolytes consisted of 0.5 M LiI, 0.05 M I_2, and 0.5 M tertbutylpyridine in acetonitrile.

2.3. Characterization of DSSCs

A field emission scanning electron microscopy (JSM-6700F, JEOL Inc., Japan) was used to observe the morphology and cross-sectional profiles of the anodic TiO_2 nanotube arrays. X-ray diffraction (XRD) was employed to investigate the phase structure of the TiO_2 powders, using a D/max 2400 X Series X-ray diffractometer. The X-ray radiation source used was Cu Kα, obtained at 40 kV, 100 mA and the scanning speed was 10°/min at a step of 0.02°. The current–voltage (*I–V*) curves of DSSCs were recorded by a Keithley SMU 2400 Source Measure unit. The EIS and OCVD measurements were obtained by using a Corrtest CS electrochemical workstation. The fabricated cells were illuminated under a solar simulator (Xenon lamp, AM 1.5, 100 mW cm^{-2}, Beijing Changtuo Technology Co., Ltd., CHF-XM-500W, calibrated by a standard crystalline silicon solar cell).

3. Results and discussions

Fig. 1(a) shows the SEM image of the morphology of the as-anodized TiO_2 nanotube arrays at present conditions. The nanotube diameter is about 120 nm, and the tube walls are smooth. In addition, for 3-h anodic oxidation at present conditions, the TiO_2 nanotubes can come to a length of 40–50 μm as shown in the inserted image at the bottom left of Fig. 1(a). This fast speed of tube growth might be ascribed to the existence of water in the organic electrolyte [11]. After sonification and grinding, the nanotube length would become shorter as shown in the inserted SEM image at the top left of Fig. 1(a). The tube length is reduced to about 4 μm or below. Fig. 1(b) shows the XRD patterns of the anodic TiO_2 nanotube powders and P25 powders. It can be observed that after calcination at 450 °C for 4 h, the anodic TiO_2 nanotubes become pure anatase, while P25 powders are mainly anatase phase with a small amount of detective rutile phase.

Fig. 2(a) shows the current–voltage (*I–V*) curves of the assembled DSSCs with different concentrations of the anodic TiO_2 nanotubes. Fig. 2(b) and (c) depicts the effect of the concentrations of the anodic TiO_2 nanotubes on the photovoltaic parameters of DSSCs. It can be observed a highest short circuit current density (I_{sc}) of 8.33 mA cm^{-2} and a maximum energy conversion efficiency (η) of 3.11% can be obtained at an incorporation level of 10 wt% of nanotubes. The I_{sc} and η at 10 wt% are enhanced by 22% and 11% respectively as compared to those at 0 wt%. With further increasing

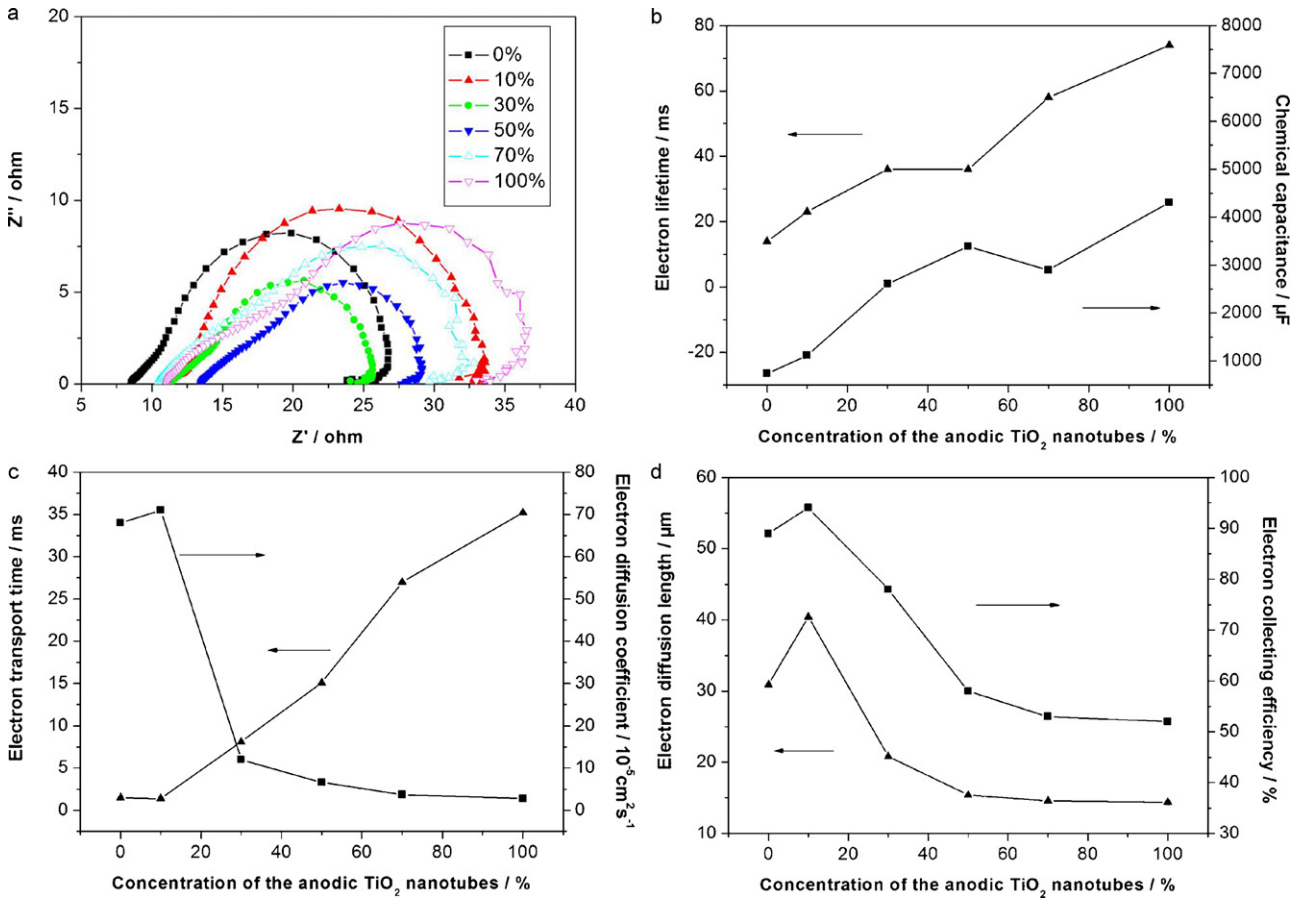

Fig. 3. (a) EIS Nyquist plots of the DSSCs as a function of the concentration of the anodic TiO_2 nanotubes; (b) curves of electron lifetime and chemical capacitance as a function of the concentration of the anodic TiO_2 nanotubes; (c) curves of electron transport time and electron diffusion coefficient as a function of the concentration of the anodic TiO_2 nanotubes; (d) curves of electron diffusion length and electron collecting efficiency as a function of the concentration of the anodic TiO_2 nanotubes.

Table 2
Electron properties of the DSSCs.

Samples	K_{eff} (s^{-1})	τ (ms)	t (ms)	R_c (Ω)	R_t (Ω)	D_{eff} ($cm^2\ s^{-1}$)	L_F (μm)	L_n (μm)	C_μ (μF)	η_{cc} (%)
0%	70.65	14	1.5	16.1	1.7	6.8e−4	10	30.9	739	89
10%	44.16	23	1.4	19.7	1.2	7.1e−4	10	40.4	1117	94
30%	27.44	36	8.1	11.1	2.5	1.2e−4	10	20.8	2609	78
50%	27.44	36	15.1	10.5	4.4	6.6e−5	10	15.4	3390	58
70%	17.13	58	27.0	14.2	6.6	3.7e−5	10	14.6	2900	53
100%	13.59	74	35.2	16.6	7.9	2.8e−5	10	14.4	4310	52

the concentrations of the nanotubes, these above two parameters keep decreasing. As to the open circuit voltage (V_{oc}) and the fill factor (FF), the concentrations of the anodic TiO_2 nanotubes have little influence on them. Thus, variation of η with tuning the concentration of the anodic TiO_2 nanotubes is mainly due to the variation of I_{sc}. It can be concluded preliminarily that the highest short circuit current obtained at 10 wt% might mainly contribute to the maximum energy conversion efficiency at this point. The detailed photovoltaic characteristics of DSSCs are shown in Table 1.

The electron transport and recombination properties of the assembled DSSCs are examined by EIS under illumination at AM 1.5 conditions. The magnitude of the alternative signal is 10 mV, and the frequency range is from 10^5 to 10^{-2} Hz. Fig. 3(a) shows the Nyquist plots of the obtained impedance data of DSSCs with different concentrations of the anodicTiO_2 nanotubes. After the data being fitted by a proper equivalent circuit [18], the derived parameters are present in Table 2. These include: the first-order reaction rate constant for the loss of electrons (K_{eff}), the lifetime of an electron ($\tau = 1/K_{eff}$), the impedance of electron transport in TiO_2 (R_t), the impedance of electron recombination with the electrolyte (R_c), chemical capacitance (C_μ) and the TiO_2 film thickness (L_F). The effective diffusion coefficient (D_{eff}) and the diffusion length (L_n) are calculated using the following equations [19,20]:

$$D_{eff} = \left(\frac{R_c}{R_t}\right)\left(\frac{L_F^2}{\tau}\right) \quad (1)$$

$$L_n = \sqrt{\tau D_{eff}} \quad (2)$$

The mean electron transport time (t) through TiO_2 films can be obtained by the equation [21]:

$$\frac{t}{\tau} = \frac{R_t}{R_c} \quad (3)$$

Because the electrons may diffuse forward and recombine with the electrolyte, the electron collecting rate at the FTO substrate is as follows:

$$\frac{1}{\tau_{cc}} = \frac{1}{t} - \frac{1}{\tau} \quad (4)$$

where τ_{cc} is the time constant of electron collection. Accordingly, the electron collecting efficiency can be written as [22]:

$$\eta_{cc} = \frac{1/\tau_{cc}}{1/t} = 1 - \frac{t}{\tau} \quad (5)$$

Fig. 3(b) depicts the correlation among the electron lifetime, the chemical capacitance and the concentration of the anodic TiO_2 nanotubes. The anodic TiO_2 nanotubes serve here not only as transport paths but also as trapping sites preventing electrons recombining with the electrolyte. Therefore, the electron lifetime increases with increasing the concentration of the anodic TiO_2 nanotubes. The introduction of the anodic TiO_2 nanotubes can enlarge the electron lifetime in the TiO_2 films. The chemical capacitance gives the total density of free electrons in the conduction band and the localized electrons in the trap sites [23]. The increase of C_μ might be related to the combining effects of the anodic TiO_2 nanotubes on both electron recombination and transport. Fig. 3(c) shows the curves of the electron transport time and the electron diffusion coefficient as a function of the concentration of the anodic TiO_2 nanotubes. It is observed that the electron transport time at a blending level of the 10 wt% anodic TiO_2 nanotubes is short as compared to that at 0 wt% and above 10 wt%, the electron transport time has a trend of becoming large. Furthermore, it can also be seen in Fig. 3(c) that the electron diffusion coefficient achieves the highest at 10 wt%. Above 10 wt%, the electron diffusion coefficient decreases with the nanotube concentration. Thus, it can be inferred that electrons can transport fastest in the TiO_2 films at 10 wt% nanotube concentration. Fig. 3(d) shows that both the electron diffusion length L_n and the electron collecting efficiency η_{cc} reach the maxima at 10 wt%. It is known that the electron diffusion length and the electron collecting efficiency are related to the electron transport and recombination from Eqs. (2) and (5). Therefore, the values of L_n and η_{cc} reflect the combining effects of the electron transport and the electron recombination.

The above experiment observations can be explained as following: when a small amount of the anodic TiO_2 nanotubes is blended into the P25 system, it can facilitate faster electron transport and at the same time retard electron recombination. This can be demonstrated by the facts that the electron transit time in 10 wt% system (1.4 ms) is smaller than that in the pure P25 system (1.5 ms), the electron diffusion coefficient in 10 wt% ($7.1e{-}4\ cm^2\ s^{-1}$) is larger than that in the pure P25 system ($6.8e{-}4\ cm^2\ s^{-1}$), and in particular, the electron lifetime in 10 wt% system (23 ms) is much longer than that in the pure P25 system (14 ms). Thus, L_n and η_{cc} can achieve the maximum values at 10 wt%. However, when the amount of anodic TiO_2 is over a critical value (10 wt% in this case), the disordered anodic TiO_2 nanotubes distributed in the P25 system might act as trap centers to be harmful for electron transportation to the FTO electrode. It would be difficult for electrons to find quick paths to the FTO substrate, which is proven by the increased electron transport time and the decreased electron diffusion coefficient when the concentration is over 10 wt%. Although the electron recombination is less, the prolonged electron transport time might be the key element to control the values of L_n and η_{cc}. Thus, L_n and η_{cc} keep decreasing when the nanotube concentrations are above 10 wt%. The electron transport process in TiO_2 is schematically shown in Fig. 4. As shown in Fig. 4(a), the anodic TiO_2 nanotubes at a blending level of 10 wt% might be dispersed uniformly in the P25 particles. These separated TiO_2 nanotubes dispersed in P25 particles can supply shorter paths for electron transport than the twisted inter-connected P25 particles. However, when the concentration of the blending TiO_2 nanotubes is over 10 wt% as shown in Fig. 4(b), the increased TiO_2 nanotubes might be dispersed disorderly in P25 particles. The higher concentration of disordered TiO_2 nanotubes might result in longer paths for electrons to transport to the FTO electrode, and even dead cycles for electron transport. Due to the electron properties of transport and recombination, the I_{sc} and η obtain the highest values at 10 wt%. In addition to the prolonged electron transport time, the decreased I_{sc} and η above 10 wt% might be also due to sacrificing surface areas to absorb dye moleculars.

The electron recombination kinetics is also studied by the OCVD method. After turning off the AM 1.5 simulated sunlight, the electron density in the TiO_2 conduction band decreases, and thus the V_{oc}

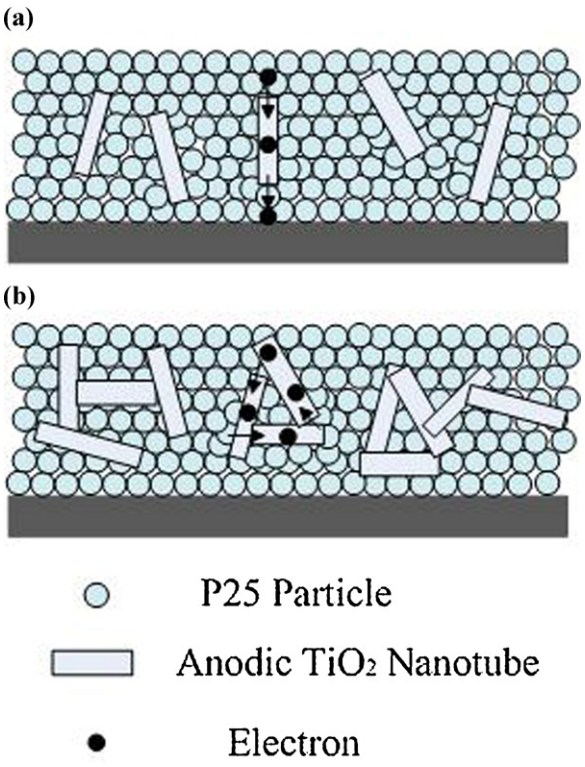

Fig. 4. Schematic diagrams of the electron transport behaviors in the TiO_2 films at a concentration of 10 wt% (a) and over 10 wt% (b) when the anodic TiO_2 nanotubes are blended into the P25 films.

decay sharply due to the electron recombination, with the V_{oc} decay rate determined by the electron recombination rate. The electron lifetime can be obtained by the below equation [24]:

$$\tau_n = \left(\frac{-k_B T}{e}\right)\left(\frac{dV_{oc}}{dt}\right)^{-1} \quad (6)$$

where k_B is the Boltzmann constant, T is the temperature, e is the positive elementary charge, and dV_{oc}/dt is the derivative of V_{oc} transient. The correlation between the calculated τ_n and V_{oc} is shown in Fig. 5. The larger τ_n means slower recombination. It can be observed in Fig. 5 that the P25 system blended with anodic TiO_2 nanotubes has larger τ_n as compared to the pure P25 system, that is to say, the P25 system blended with anodic TiO_2 nanotubes has slower recombination as compared with the pure P25 system. With increasing the concentration of the blending TiO_2 nanotubes, the τ_n has a trend of becoming larger. These results agree well with those obtained from the EIS measurement. When the anodic TiO_2 nanotubes are blended into the P25 particles, the electron recombination can be restricted, and thus the average electron lifetime τ derived by EIS can also be enlarged as discussed before. The enlargement of τ_n can be explained by an internal radial electric field that is developed within the walls of the TiO_2 nanotubes, when increasing the concentration of the blending TiO_2 nanotubes. This internal electric field can drive the injected electrons away from the surface of TiO_2 nanotubes, preventing the electron recombination with the electrolyte and the exited dye molecules [3].

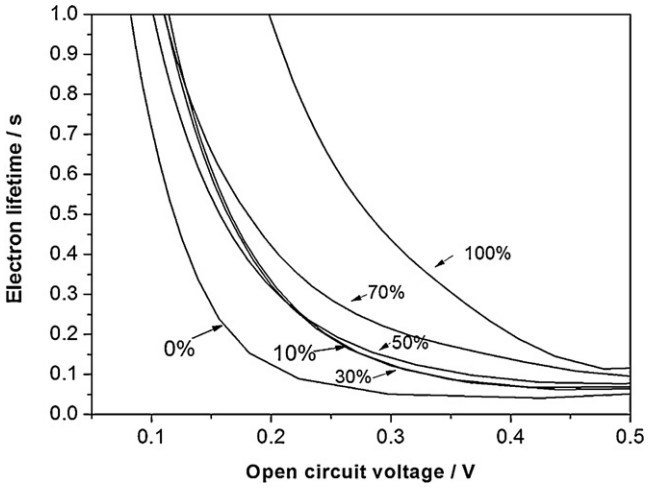

Fig. 5. The correlation between electron lifetime and open circuit voltage obtained from the OCVD method.

4. Conclusions

In this work, charge transport and recombination in DSSCs based on hybrid films of TiO_2 particles/anodic TiO_2 nanotubes are investigated by using the EIS and OCVD methods. The combining effects of electron transport and recombination contribute to the electron collecting efficiency and the electron diffusion length affecting the short circuit current and the energy conversion efficiency. The reasons have been explored why only a small amount of the blending 1D TiO_2 nanostructures (10 wt% anodic TiO_2 nanotubes in this case) into TiO_2 particle-based films can enhance the performance of DSSCs, and why excessive blending 1D TiO_2 nanostructures (over 10 wt% nanotubes in this case) deteriorates the performance of DSSCs from the aspects of charge transport and recombination. These findings will be helpful for stimulation of searching new ways to retard electron recombination and facilitate electron transport, in order to increase the photovoltaic performances of DSSCs.

Acknowledgements

This work was supported by the Ministry of Science and Technology of China through 863-project under grant 2009AA03Z218, the Major Program of the National Natural Science Foundation of China under Grant No. 90923012, and the Research Fund for the Doctoral Program of Higher Education of China under grant 200806980023. The authors would also like to thank National Research Foundation, Singapore for partial support through a project NRF-CRP-G-2007-01.

References

[1] B. O'Regan, M. Gratzel, Nature 353 (1991) 737–740.
[2] M. Gratzel, Nature 414 (2001) 338–344.
[3] C. Xu, P.H. Shin, L. Cao, J. Wu, D. Gao, Chem. Mater. 22 (2010) 143–148.
[4] T. Stergiopoulos, A. Valota, V. Likodimos, Th. Speliotis, D. Niarchos, P. Skeldon, G.E. Thompson, P. Falaras, Nanotechnology 20 (2009) 365601–365609.
[5] E.J.W. Crossland, M. Nedelcu, C. Ducati, S. Ludwigs, M.A. Hillmyer, U. Steiner, H.J. Snaith, Nano Lett. 9 (2009) 2813–2819.
[6] T.S. Kang, A.P. Smith, B.E. Taylor, M.F. Durstock, Nano Lett. 9 (2009) 601–606.
[7] T.R.B. Foong, Y. Shen, X. Hu, A. Sellinger, Adv. Funct. Mater. 20 (2010) 1390–1396.
[8] J.H. Yoon, S.R. Jang, R. Vittal, J. Lee, K.J. Kim, J. Photochem. Photobiol. A: Chem. 180 (2006) 184–188.
[9] S.H. Kang, S.H. Choi, M.S. Kang, J.Y. Kim, H.S. Kim, T. Hyeon, Y.E. Sung, Adv. Mater. 20 (2008) 54–58.
[10] I.C. Flores, J.N.d. Freitas, C. Longo, M.A.D. Paoli, H. Winnischofer, A.F. Nogueira, J. Photochem. Photobiol. A: Chem. 189 (2007) 153–160.
[11] H.E. Prakasam, K. Shankar, M. Paulose, O.K. Varghese, C.A. Grimes, J. Phys. Chem. C 111 (2007) 7235–7241.
[12] J. Wang, L. Zhao, V.S.Y. Lin, Z. Lin, J. Mater. Chem. 19 (2009) 3682–3687.
[13] J. Wang, Z. Lin, Chem. Mater. 22 (2010) 579–584.
[14] J. Wang, Z. Lin, Chem. Mater. 20 (2008) 1257–1261.
[15] J. Wang, Z. Lin, J. Phys. Chem. C 113 (2009) 4026–4030.
[16] W. Que, A. Uddin, X. Hu, J. Power Sources 159 (2006) 353–356.
[17] S. Ito, T.N. Murakami, P. Comte, P. Liska, C. Gratzel, M.K. Nazeeruddin, M. Gratzel, Thin Solid Films 516 (2008) 4613–4619.
[18] Q. Wang, S. Ito, M. Gratzel, F. Fabregat-Santiago, I. Mora-Sero, J. Bisquert, T. Bessho, H. Imai, J. Phys. Chem. B 110 (2006) 25210–25221.

[19] M. Adachi, M. Sakamoto, J. Jiu, Y. Ogata, S. Isoda, J. Phys. Chem. B 110 (2006) 13872–13880.
[20] S. Nakade, M. Matsuda, S. Kambe, Y. Saito, T. Kitamura, T. Sakata, Y. Wada, H. Mori, S. Yanagida, J. Phys. Chem. B 106 (2002) 10004–10010.
[21] P.T. Hsiao, Y.L. Tung, H. Teng, J. Phys. Chem. C 114 (2010) 6762–6769.
[22] J. Van de Lagemaat, N.G. Park, A.J. Frank, J. Phys. Chem. B 104 (2002) 2044–2052.
[23] R. Kern, R. Sastrawan, J. Ferber, R. Stangl, J. Luther, Electrochim. Acta 47 (2002) 4213–4225.
[24] J. Bisquert, A. Zaban, M. Greenshtein, I. Mor-Sero, J. Am. Chem. Soc. 126 (2004) 13550–13559.